MICROMECHANICS OF INTRA-LAMINAR HYBRID LAMINA WITH HOLLOW FIBRES: A RVE MODEL

Giuseppe Romano [1], Yang Yang [1], Zhenmin Zou [1], Prasad Potluri [2, 3], Kali Babu Katnam [1, 2 *]

[1] Department of Mechanical, Aerospace and Civil Engineering, The University of Manchester, UK
[2] Northwest Composites Centre, The University of Manchester, UK
[3] Department of Materials, The University of Manchester, Manchester, UK
* Corresponding author (Kali-Babu.Katnam@manchester.ac.uk)

Keywords: Fibre hybrid composites, RVE modelling, hollow glass fibres, micro-stress fields

ABSTRACT

In this work, unidirectional composite laminae with intra-laminar fibre hybridisation (i.e. two fibre types within a matrix) are studied to understand the influence of solid and hollow glass fibre content on the homogenised specific lamina properties of and the matrix micro-stress fields in carbon/solid-E-glass/epoxy and carbon/hollow-E-glass/epoxy laminae. A 3D representative volume element (RVE) model is developed for the micromechanical analysis of unidirectional composite laminae with intra-laminar fibre hybridisation by considering random fibre distribution. The random sequential expansion (RSE) algorithm is modified to generate fibre hybrid microstructures. The RVE model is validated with analytical models. Using the RVE model, carbon/solid-E-glass/epoxy and carbon/hollow-E-glass/epoxy fibre hybrid laminae are studied. The results show that the intra-laminar hybridisation of carbon/epoxy laminae with hollow glass fibre content can affect the density and significantly alter the homogenised specific transverse lamina properties, while the reduction in the specific longitudinal elastic properties is negligible. Moreover, the RVE models with random fibre microstructures show that the presence of hollow glass fibres can considerably alter the matrix micro-stress fields in carbon/hollow-E-glass/epoxy laminae when compared to the micro-stress fields in carbon/solid-E-glass/epoxy laminae.

1 INTRODUCTION

Polymer-matrix composite laminates have become increasingly popular in various industries (e.g. automotive and aerospace) because of their high strength-to-weight and stiffness-to-weight ratios. However, composite laminates are prone to impact-induced damage and have relatively poor post-impact performance. To address some of the disadvantages of the conventional composite laminates, two or more fibres can be combined to produce fibre hybrid composites (FHCs), such as inter-laminar (with different single fibre-based laminae) or intra-laminar (with more than one fibre-based laminae) hybrid laminate [1,2]. For example, the issues related to the impact damage resistance and post-impact damage tolerance in composite laminates are addressed with fibre hybridisation (e.g. intra-yarn, inter-yarn and/or inter-lamina hybridisation [3]). Yarn-level hybridization, via commingling and core wrapping, is a cost-effective solution to improve the impact and post-impact damage performance of 2D woven laminates by manipulating micro-damage modes and inducing energy dissipation mechanisms [3–5]. Moreover, hollow glass fibres can be used to “heal” the damaged composite structure, and improve specific strength, stiffness, and post-impact damage performance in composite structures [6,7]. In this context, carbon/epoxy hybrid laminates with intra-laminar hollow fibre content can be explored to tailor the specific properties and, offer opportunities to introduce microstructures for additional functionalities such as healing.

Numerous computational studies have been carried out to examine the mechanical behaviour of hybrid laminates made of synthetic fibres. These investigations have looked into various aspects, including the inter-laminar hybridization of Kevlar-based laminates with E-glass [8], carbon fibre-based laminates with Kevlar [9], and the intra-laminar hybridisation of carbon fibre-based laminae with E-glass [10,11]. These studies have predominantly employed computational micromechanics of composites through the use of representative volume element (RVE) models [12] with periodic boundary conditions [13]. However, there is currently a lack of computational studies focusing on the intra-laminar hybridization of carbon/epoxy laminates incorporating hollow glass fibres. To address this research gap, a computational study was conducted to investigate the effect of fibre hybridization on both the homogenized specific properties of the laminate and the distribution of micro-stress within the laminate. Specifically, the study examined the intra-laminar hybridization of unidirectional carbon/epoxy laminae with both solid and hollow glass fibres. To simulate the intra-laminar fibre hybrid microstructures, an RVE model was developed using a modified random sequential expansion algorithm [14], which was implemented utilizing Python and ABAQUS/standard.

2 METHODOLOGY

2.1 RVE Modelling

It is well recognised that the relationship between the continuum properties of a material neighbourhood and its microstructure and micro-constituents is important for heterogeneous materials, especially for fibre-reinforced polymer composites with heterogeneity at the microscale. The notion of a representative volume element is used as the physical basis for the transition from the microscale to the macroscale, and the associated boundary-value problem is formulated in terms of field variables by imposing traction and/or displacement boundary conditions [15,16]. Computational micromechanics plays a major role to understand the deformation processes at the microscale as well as to estimate the homogenised properties of composite laminae with intra-laminar fibre hybrid microstructure. In this regard, a 3D RVE model is developed for fibre hybrid unidirectional carbon/epoxy laminae. Two fibre hybrid cases are considered: carbon/solid-E-glass/epoxy and carbon/hollow-E-glass/epoxy. In Fig. 1, a hybrid laminate with intra-laminar fibre hybridisation, with solid and hollow fibres (Fig.1a), and a 3D RVE with random fibre distribution for the micromechanical analysis of laminates with intra-laminar fibre hybridisation (Fig. 1b) are shown. The rectangular coordinate system (x_i) in Fig. 1 is aligned with the principal material coordinate system. To simplify the model, the fibres within the lamina are assumed continuous, homogeneous, transversely isotropic, and defect-free with circular cross-sections. The epoxy matrix is assumed homogeneous, isotropic, and void-free. It is assumed that both carbon and glass fibres have a perfect fibre-matrix interface. It is also assumed that the variation in the material properties and diameter of each fibre type is negligible. In addition, the fibres and matrix are linear elastic.

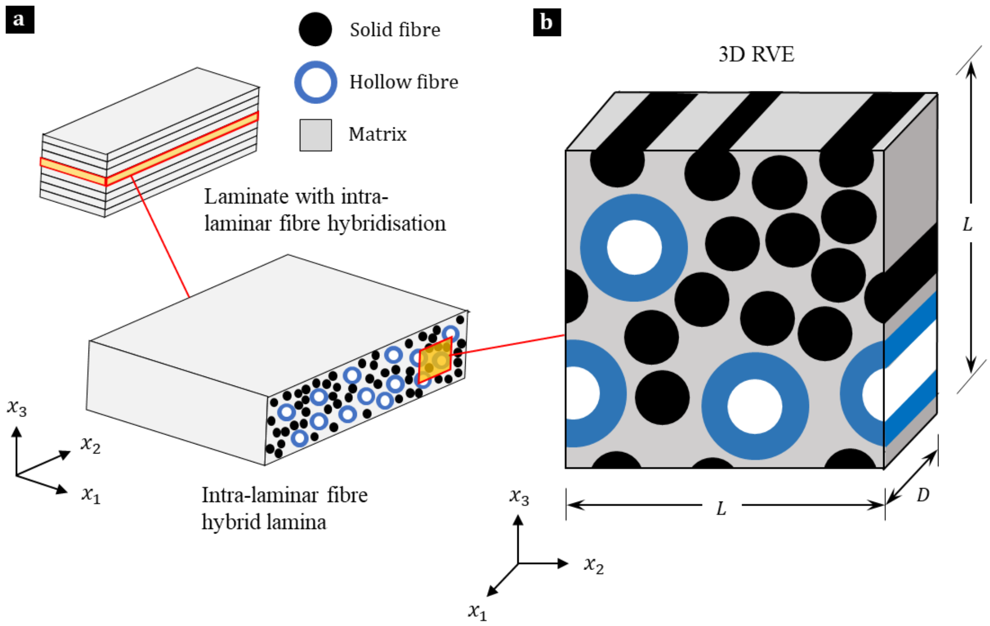

Figure 1: The RVE modelling approach for fibre hybrid lamina: (a) laminate with intra-laminar hybridisation, and (b) the microstructure of solid/hollow/epoxy fibre hybrid lamina

Considering a random fibre distribution within the hybrid lamina, the microstructure of the RVE is generated using a modified random sequential expansion (RSE) algorithm. To achieve the targeted fibre volume fraction, the RSE algorithm is modified to disperse carbon and glass fibres. The modified RSE algorithm prioritises the placement of the large fibres within the RVE domain, leaving enough space for the small fibres while meeting the volume fraction targets for both types of fibres. The algorithm also assures geometric periodicity at the RVE boundaries for carbon/hollow-E-glass/epoxy, as illustrated schematically in Fig.1b, in order to apply mesh-based period displacement boundary conditions. In the current study, the RVE model is applied to study unidirectional carbon/solid-E-glass/epoxy and carbon/hollow-E-glass/epoxy hybrid composite laminae. The total fibre volume fraction of 0.60 is considered, while the individual fibre volume fractions of carbon (V_{fC}) and solid glass (V_{fG}) or hollow glass fibres (V_{fH}) are 0.15 and 0.45, respectively.

To generate fibre hybrid microstructures for the 3D RVE models, the random sequential expansion algorithm, developed by Yang et al., 2013 [14] based on the NNA algorithm [17] with a reduced number of parameters, is modified as shown in Fig. 2, where the large inclusions are hollow fibres and the small inclusions are solid fibres. In step 1, as unidirectional fibres are only considered, a square domain, which is the size of the RVE, is defined and a random point within the domain is generated and used as the centre for the first large diameter fibre (Fig. 2a). In step 2, a second large fibre is placed with a random distance, ranging between a minimum (δ_{min}) and maximum (δ_{max}) distance from the centre of the first fibre generated in step 1, and with a random angle (θ_1), ranging from 0 to 2π, from the first fibre. In step 3, step 2 is repeated to place the third fibre (Fig. 2c). In step 4, steps 2-3 are repeated until no new fibres can be placed around the first fibre (Fig. 2d). In step 5, the steps 2-4 are repeated on the second fibre (Fig. 2e). In step 6, the steps 2-6 are repeated until no more large fibre can be placed within the RVE domain. To generate the small fibre content, large fibres are randomly removed until the targeted large fibre volume fraction is achieved. In step 7, steps 2-6 are repeated to place the small fibres until the targeted small fibre volume fraction is attained. In addition, the algorithm checks that no overlapping of the fibres is happening. If a partial fibre is generated near the edge, the remaining fibre is generated on the opposite edge. A minimum distance from the edge is preserved to avoid too sharp edges, which result in excessively distorted mesh elements.

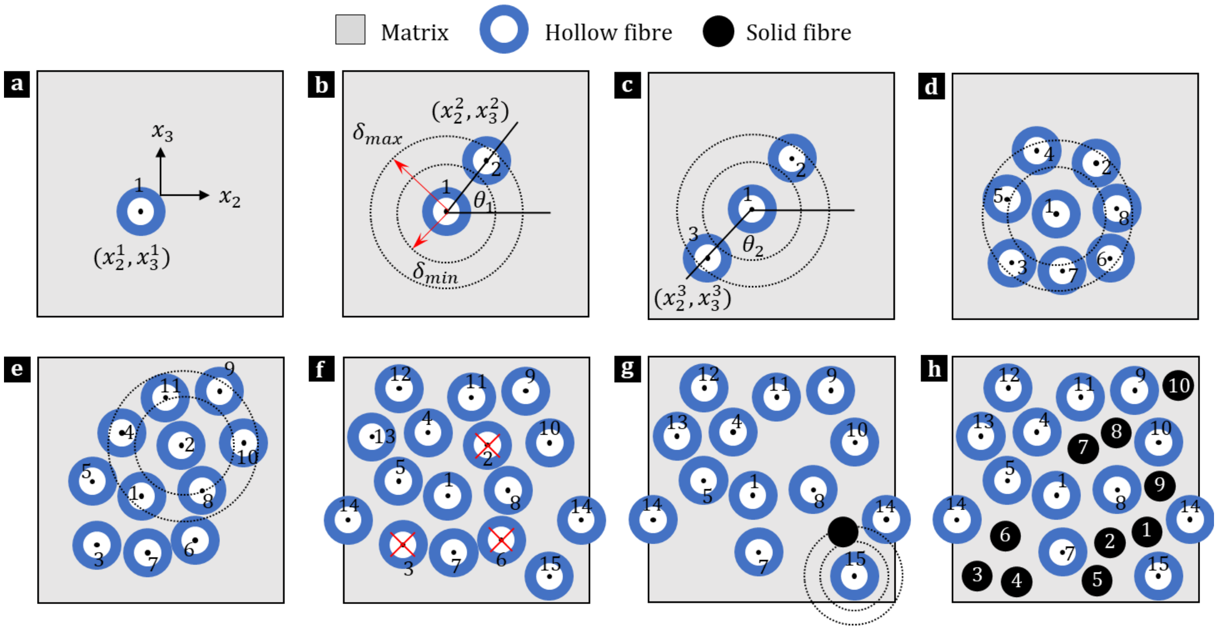

Figure 2: The modified RSE algorithm used to generate the microstructures with fibre hybridisation

Using Python and Abaqus/Standard, the RVE model is implemented by using the finite element method. The micro-stress/strain fields and the homogenised material properties are obtained by imposing displacement-based periodic boundary conditions. For the current investigation, the material properties used in the RVE models are given in Table 1. In addition, the diameters of solid E-glass (12 μm), hollow E-glass (12 μm) and carbon (7 μm) fibres are assumed. A 20% hollowness is considered for the inner diameter of the hollow E-glass. The minimum inter-fibre distance is fixed at 7% of the carbon fibre diameter, while the maximum is 14% of the carbon fibre diameter. The RVE size is determined by taking into account the large fibre diameter as the characteristic length of the micro-constituents. To ensure that the RVE is significantly larger than the fibre diameters, the size of the RVE (perpendicular to the fibre direction) is set to 10 times the diameter of the large fibre. Since the fibres are unidirectional, a thickness equivalent to the mean value of the global mesh size adopted is utilized for the thickness of the RVE (along the fibre direction). Linear brick elements with reduced integration (C3D8R), and full integration wedge elements (C3D6) are employed to mesh the matrix and fibres, respectively. To establish mesh convergence, a study is conducted to determine the appropriate average element size for the RVE. The RVEs are meshed with an element size much smaller than the radius of the small fibre, and only one element is used along the thickness direction.

Table 1: The material properties of the fibres and matrix used in the RVE models of carbon/solid-E-glass/epoxy and carbon/hollow-E-glass/epoxy laminae [11]

	E_{11} [GPa]	$E_{22} = E_{33}$ [GPa]	$G_{12} = G_{13}$ [GPa]	G_{23} [GPa]	$\nu_{12} = \nu_{13}$	ν_{23}	ρ [g/cm^3]
E-glass	72.4	72.4	30.2	30.2	0.2	0.2	2.54
Carbon	263	19	`27.6	7.04	0.2	0.35	1.78
Epoxy	3.5	3.5	1.29	1.29	0.35	0.35	1.29

2.2 Periodic boundary conditions

The homogenised properties of fibre hybrid laminae can be estimated by using the unweighted volume averages of the micro-stresses and micro-strains within the RVE. However, the estimated properties depend on the type of boundary conditions imposed on the RVEs. The linear displacement (uniform macro-strain) and uniform traction (uniform macro-stress) boundary conditions provide the upper and lower bounds of the homogenised properties. The strain energies predicted by imposing uniform traction conditions, periodic displacement conditions and linear displacement conditions satisfy the inequality $U_t \leq U_p \leq U_u$ (where U_t, U_p, U_u are the strain energies obtained by imposing uniform traction, period displacement, and linear displacement boundary conditions) when the same average strain is considered for each case. As the linear displacement conditions overestimate (and the uniform traction conditions underestimate) the effective properties, the periodic displacement conditions are used for the RVE models. The periodic displacement conditions are imposed by using Eq. 1 [13,18]. Although the application of the linear displacement boundary conditions generally does not guarantee periodic traction conditions (similarly, the uniform traction conditions do not guarantee the periodic displacement conditions) at the boundaries, it can be shown that the periodic displacement conditions guarantee periodic traction conditions.

$$u_i(\boldsymbol{x} + \Delta\boldsymbol{x}) - u_i(\boldsymbol{x}) = \hat{\varepsilon}_{ij}\Delta x_j \qquad (i,j = 1,2,3) \tag{1}$$

In Eq. 1, u_i is the displacement in the x_i direction, $\boldsymbol{x} + \Delta\boldsymbol{x}$ and $\boldsymbol{x}$ are the position vectors of the points on the opposite faces of the RVE, and $\hat{\varepsilon}_{ij}$ is the macro-strain component.

2.4 Homogenization

With the periodic displacement conditions (Eq. 1), the homogenised lamina properties are obtained by applying a uniform macro-strain state and then calculating the unweighted volume average of the micro-stresses and micro-stains within the RVE. Applying Gauss's divergence theorem and the condition $\sigma_{ij,j} = 0$ for the micro-stress field (i.e. divergence-free), the unweighted volume average of the micro-stress is obtained, by using Eq. 2, from the reaction forces at the reference nodes, which are used to impose the periodic boundary conditions. In Eq. 2, $\hat{\sigma}_{ij}$ is the homogenised macro-stress, $\hat{\varepsilon}_{ij}$ is the homogenised macro-strain, V is the RVE volume, ∂V is the RVE boundary, n_i is the outward normal at the boundary, $(R_i)_j$ is the reaction force (which is the resultant traction on the surface with the outward normal in the x_j-direction) at the reference node in the x_i direction, A_j is the area of the boundary surfaces with the outward normal in the x_j-direction, and Γ_i the length of the boundary edge with the outward normal in the x_i-direction.

$$\hat{\sigma}_{ij} = \frac{1}{\Omega}\int_{\Omega} \sigma_{ij} d\Omega = \int_{\partial\Omega=\Upsilon} \sigma_{ik} n_k x_j d\Upsilon = \frac{(R_i)_j}{A_j} \quad \text{(no summation over the index } j\text{)} \quad (2.1)$$

$$\hat{\varepsilon}_{ij} = \frac{1}{\Omega}\int_{\Omega} \varepsilon_{ij} d\Omega = \frac{1}{2\Omega}\int_{\partial\Omega=\Upsilon} (u_i n_j + u_j n_i) d\Upsilon = \frac{u_i \Gamma_i + u_j \Gamma_j}{\Gamma_i \Gamma_j} \quad (i \text{ and } j \text{ are not dummy}) \quad (2.2)$$

Using the macro-strain state, six independent loading conditions, i.e. normal and shear loading along longitudinal and transverse directions) are imposed on the 3D RVE model and the homogenised lamina properties (i.e. $\hat{E}_{11}$, $\hat{E}_{22}$, $\hat{E}_{33}$, $\hat{G}_{12}$, $\hat{G}_{13}$, $\hat{G}_{23}$, $\hat{\nu}_{12}$, $\hat{\nu}_{13}$, $\hat{\nu}_{23}$) are obtained.

3 RESULTS AND DISCUSSION

3.1 Model validation

Using the 3D RVE model, the homogenised properties of unidirectional E-glass/epoxy, carbon/epoxy and carbon/E-glass/epoxy laminae are obtained and compared with the properties estimated by the rule of mixtures and the modified Halpin-Tsai equations [11]. The RVE microstructures of the E-glass/epoxy and carbon/epoxy laminae are generated with a fibre volume fraction of ~0.60. For the carbon/E-glass/epoxy hybrid lamina, the RVE microstructures are generated with a carbon fibre volume fraction (V_{fC}) of ~0.15 and an E-glass fibre volume fraction (V_{fG}) of ~0.45. The diameter of carbon and E-glass are 7 μm and 12 μm. Five microstructures are generated for each lamina and the average homogenised properties (with standard deviation) are included in Tables 2-4. Using the analytically estimated properties, the homogenised properties of E-glass/epoxy and carbon/epoxy laminae are compared and given in Tables 2-3, and that of carbon/E-glass/epoxy lamina in Table 4. The variation (%) to the analytical data in absolute value in Tables 2-4 shows that the homogenised properties obtained from the 3D RVE model are in agreement with those estimated from the analytical models. The variation in the in-plane shear moduli is relatively high (17-24%), whereas the variation in the major Poisson's ratio is negligible.

Table 2: The comparison of the homogenised lamina properties of carbon/epoxy lamina (with $V_{fC} \approx 0.60$) using the RVE and analytical models [11].

	$\hat{E}_{11}$ [GPa]	$\hat{E}_{22} = \hat{E}_{33}$ [GPa]	$\hat{G}_{12} = \hat{G}_{13}$ [GPa]	$\hat{G}_{23}$ [GPa]	$\hat{\nu}_{12} = \hat{\nu}_{13}$	$\hat{\nu}_{23}$
RVE	158.63 ± 0.00	8.95 ± 0.03	5.18 ± 0.05	3.15 ± 0.01	0.25 ± 0.00	0.44 ± 0.00
Analytical	159.20	8.61	4.41	3.06	0.26	0.41
Variation (%)	0.36	3.95	17.46	2.94	3.85	8.14

Table 3: The comparison of the homogenised lamina properties of E-glass/epoxy lamina (with $V_{fG} \approx 0.60$) using the RVE and analytical models [11].

	$\hat{E}_{11}$ [GPa]	$\hat{E}_{22} = \hat{E}_{33}$ [GPa]	$\hat{G}_{12} = \hat{G}_{13}$ [GPa]	$\hat{G}_{23}$ [GPa]	$\hat{\nu}_{12} = \hat{\nu}_{13}$	$\hat{\nu}_{23}$
RVE	44.82 ± 0.00	13.98 ± 0.31	5.53 ± 0.11	5.13 ± 0.04	0.25 ± 0.01	0.38 ± 0.01

Analytical	44.84	12.21	4.47	4.32	0.25	0.40
Variation (%)	0.04	14.50	23.71	18.75	0.00	8.03

Table 4: The comparison of the homogenised lamina properties of carbon/E-glass/epoxy lamina (with $V_{fC} \approx 0.15$ and $V_{fG} \approx 0.45$) using the RVE and analytical models [11].

	$\hat{E}_{11}$ [GPa]	$\hat{E}_{22} = \hat{E}_{33}$ [GPa]	$\hat{G}_{12} = \hat{G}_{13}$ [GPa]	$\hat{G}_{23}$ [GPa]	$\hat{\nu}_{12} = \hat{\nu}_{13}$	$\hat{\nu}_{23}$
RVE	74.36 ± 0.00	12.34 ± 0.16	5.33 ± 0.14	4.40 ± 0.02	0.25 ± 0.00	0.40 ± 0.00
Analytical	73.43	11.27	4.45	4.32	0.26	0.31
Variation (%)	1.27	9.49	19.78	2.09	3.85	30.11

Table 5: The comparison of the homogenised properties of carbon/epoxy (L-1), E-glass/epoxy (L-2), carbon/solid-E-glass/epoxy (L-3) and carbon/hollow-E-glass/epoxy (L-4) laminae.

Lamina	$\hat{E}_{11}$ [GPa]	$\hat{E}_{22} = \hat{E}_{33}$ [GPa]	$\hat{G}_{12} = \hat{G}_{13}$ [GPa]	$\hat{G}_{23}$ [GPa]	$\hat{\nu}_{12} = \hat{\nu}_{13}$	$\hat{\nu}_{23}$	$\hat{\rho}$ [g/cm^3]
L-1	158.63 ± 0.00	8.95 ± 0.03	5.18 ± 0.05	3.15 ± 0.01	0.25 ± 0.00	0.44 ± 0.00	1.58
L-2	44.82 ± 0.00	13.98 ± 0.31	5.53 ± 0.11	5.13 ± 0.04	0.25 ± 0.01	0.38 ± 0.01	2.04
L-3	74.36 ± 0.00	12.34 ± 0.16	5.33 ± 0.14	4.40 ± 0.02	0.25 ± 0.00	0.40 ± 0.00	1.93
L-4	67.81 ± 0.00	10.60 ± 0.04	4.98 ± 0.04	3.67 ± 0.0	0.25 ± 0.00	0.53 ± 0.01	1.70

Table 6: The comparison of the specific homogenised properties of carbon/epoxy (L-1), E-glass/epoxy (L-2), carbon/solid-E-glass/epoxy (L-3) and carbon/hollow-E-glass/epoxy (L-4) laminae.

Lamina	$\hat{E}_{11}/\hat{\rho}$ [GPa. cm^3/g]	$\hat{E}_{22}/\hat{\rho} = \hat{E}_{33}/\hat{\rho}$ [GPa. cm^3/g]	$\hat{G}_{12}/\hat{\rho} = \hat{G}_{13}/\hat{\rho}$ [GPa. cm^3/g]	$\hat{G}_{23}/\hat{\rho}$ [GPa. cm^3/g]
L-1	100.15 ± 0.00	5.65 ± 0.02	3.27 ± 0.03	1.99 ± 0.00
L-2	21.97 ± 0.00	6.85 ± 0.15	2.71 ± 0.05	2.51 ± 0.02
L-3	38.61 ± 0.00	6.41 ± 0.08	2.77 ± 0.04	2.28 ± 0.03
L-4	39.95 ± 0.00	6.24 ± 0.02	2.93 ± 0.02	2.16 ± 0.00

3.2 Hollow fibre hybrid lamina: Homogenized properties

The comparison of the homogenised properties of carbon/epoxy and E-glass/epoxy with those of carbon/solid-E-glass/epoxy and carbon/hollow-E-glass/epoxy laminae is presented in Table 5. The fibre volume fraction is ~0.60 in carbon/epoxy (i.e. $V_{fC} \approx 0.6$) and E-glass/epoxy (i.e. $V_{fE} \approx 0.6$) laminae, whereas the total fibre volume fraction is ~0.60 in carbon/solid-E-glass/epoxy (i.e. $V_{fC} \approx 0.15$ and $V_{fE} \approx 0.45$) and carbon/hollow-E-glass/epoxy (i.e. $V_{fC} \approx 0.15$ and $V_{fH} \approx 0.45$) laminae. It is worth noting that the hollow-E-glass fibre volume fraction (V_{fH}) is the gross volume fraction (i.e. with 20% hollowness, the net fibre volume fraction is 0.36). Five RVE microstructures are generated per each lamina type and the mean homogenised properties (along with standard deviation) are reported. As can be seen in Table 5, carbon/epoxy (L-1) has the lowest effective density (1.58 g/cm^3), while E-glass/epoxy (L-2) has the highest (2.04 g/cm^3). With intra-laminar fibre hybridisation, the effective densities of carbon/solid-E-glass (L-3) and carbon/hollow-E-glass (L-4) are considerably altered. With the presence of hollow-E-glass fibres, the effective density of carbon/hollow-E-glass/epoxy lamina is comparable to that of carbon/epoxy lamina. Moreover, the longitudinal modulus ($\hat{E}_{11}$) is considerably altered with intra-laminar hybridisation. A higher longitudinal modulus is obtained for carbon/solid-E-glass/epoxy and carbon/hollow-E-glass/epoxy laminae when compared to that of E-glass/epoxy lamina.

In addition, a significant increase in the transverse Poisson's ratio ($\hat{\nu}_{23}$) is observed in carbon/hollow-E-glass/epoxy lamina because of the hollow fibre content. Overall, it can be seen that the homogenised properties are considerably altered via intra-laminar hybridisation with hollow fibres. As the effective density is lowered with hollow fibres, the specific homogenised properties are compared and presented in Table 6. In comparison with the specific properties of E-glass/epoxy lamina, it shows that the hollow fibre content can considerably lower the specific transverse elastic properties ($\hat{E}_{22}/\hat{\rho}$, $\hat{E}_{33}/\hat{\rho}$ and $\hat{G}_{23}/\hat{\rho}$), while having a negligible effect on the major Poisson's ratios ($\hat{\nu}_{12} = \hat{\nu}_{13}$). In contrast, the specific longitudinal elastic modulus ($\hat{E}_{11}/\hat{\rho}$), and the specific longitudinal shear modulus ($\hat{G}_{12}/\hat{\rho} = \hat{G}_{13}/\hat{\rho}$) are considerably increased.

3.3 Matrix micro-stress fields

From Table 5, it is observed that the transverse moduli and the transverse Poisson's ratio are considerably influenced by intra-laminar hybridisation with hollow E-glass fibres. To understand the effect of hollow fibres on the matrix micro-stresses, two loading cases that induce a matrix-dominant response are considered (i.e. transverse tension and transverse shear conditions). The transverse tensile and shear response of carbon/solid-E-glass/epoxy and carbon/hollow-E-glass/epoxy laminae are presented here. To compare the matrix stresses under transverse tension and shear loading, the microstructure is fixed for both the laminae (i.e. the same RVE microstructure is used for carbon/solid-E-glass/epoxy and carbon/hollow-E-glass/epoxy) as a diameter of 12 μm is used for both solid E-glass and hollow E-glass fibres. The von Mises stress fields are normalised with the macro-stress applied (i.e. $\sigma_{vM}/\hat{\sigma}_{22}$ and $\sigma_{vM}/\hat{\sigma}_{23}$) and are presented.

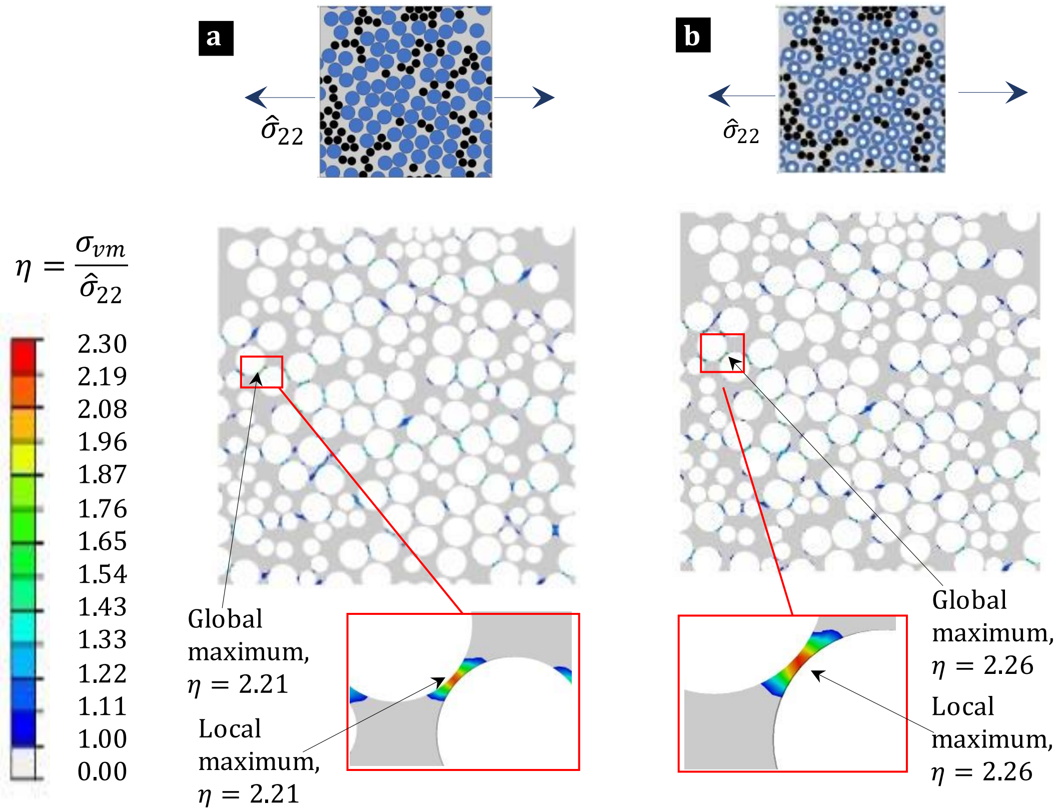

Figure 3: The normalised von Mises matrix micro-stress distribution under transverse tension (i.e. $\sigma_{vM}/\hat{\sigma}_{22}$): (a) carbon/solid-E-glass/epoxy RVE and (b) carbon/hollow-E-glass/epoxy RVE.

3.3.1 Transverse Tension

The normalised matrix stress distributions in carbon/solid-E-glass/epoxy and carbon/hollow-E-glass/epoxy laminae under transverse tension are shown in Fig. 3 (only the matrix is shown). The von

Mises stress is normalised with the macro-stress applied (i.e. $\sigma_{vM}/\hat{\sigma}_{22}$). By comparing Figs. 3a and 3b, it can be seen that the matrix stress distribution is significantly different, although the same RVE microstructure is analysed. It shows that the presence of hollow E-glass fibres redistributes the local stresses because of the hollowness. Within the RVE of carbon/E-glass/epoxy, the maximum stress amplification ($\sigma_{vM}/\hat{\sigma}_{22}$) observed is 2.21, whereas it is 2.26 (slighlty higher, ~2%) within the RVE of carbon/hollow-E-glass/epoxy. In addition, the RVE of carbon/hollow-E-glass/epoxy RVE, shown in Fig. 3b, shows that a higher volume of the matrix has a stress amplification of $\sigma_{vm}/\hat{\sigma}_{22} > 1$. In Figure 3a, the stress amplification is observed mostly between the E-glass fibres, aligning with the loading direction. From Figure 3, it is evident that the stress amplification is higher where the inter-fibre distance between the hollow fibres is smaller.

3.3.2 Transverse Shear

In Fig. 4, the normalised matrix stress distributions in carbon/solid-E-glass/epoxy and carbon/hollow-E-glass/epoxy laminae under transverse shear are presented (only the matrix is shown). The von Mises stress is normalised with the macro-stress applied (i.e. $\sigma_{vM}/\hat{\sigma}_{23}$). By comparing Figs. 4a and 4b, it is seen that the matrix stress distribution is significantly different. Similar to the observations made under transverse tension, it is evident that the presence of hollow E-glass fibres redistributes the local stresses because of the hollowness. For the same microstructure (fibre distribution) analysed, within the RVE of 5.01 (slighlty higher, ~4%) within the RVE of carbon/hollow-E-glass/epoxy.. Furthermore, the RVE of carbon/hollow-E-glass/epoxy RVE, shown in Fig. 4b, indicates that a higher volume of the matrix has a stress amplification of $\sigma_{vm}/\hat{\sigma}_{23} > 1$. In 4b, the stress amplification is observed mostly between the hollow E-glass fibres where the inter-fibre distance between the hollow fibres is small.

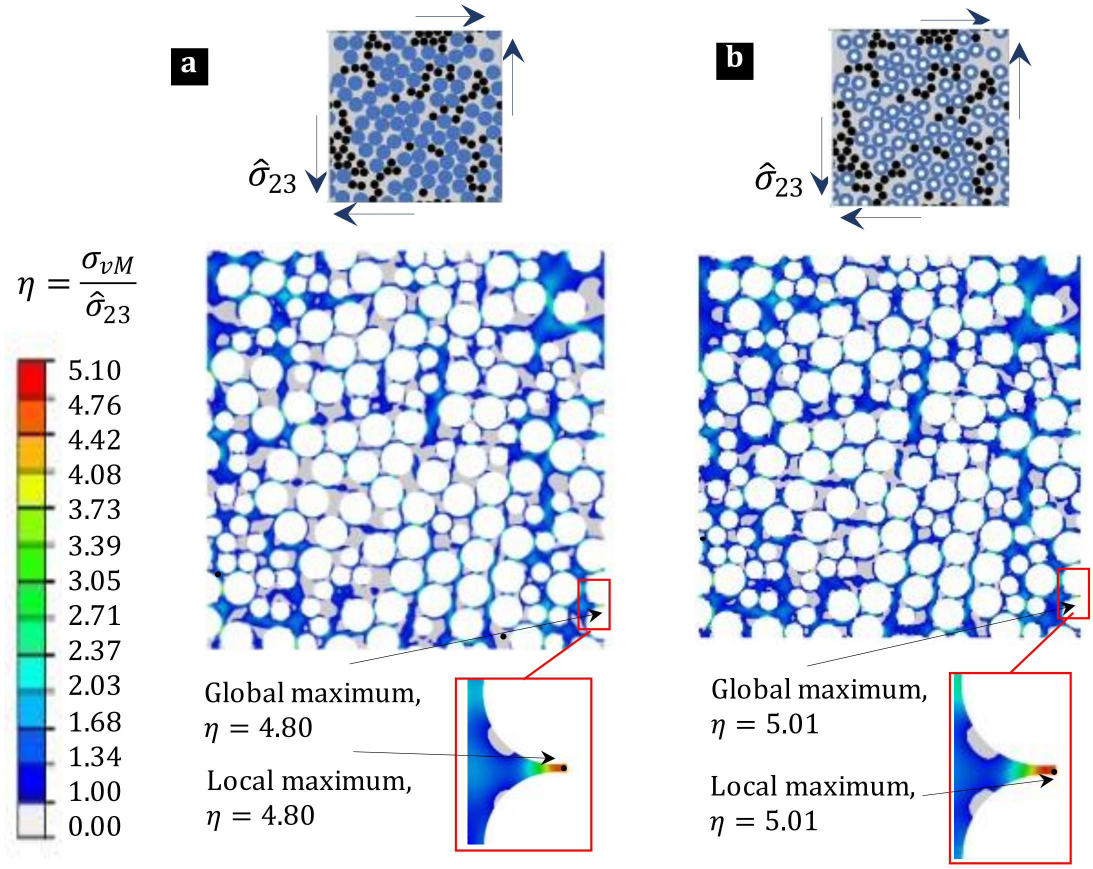

Figure 4: The normalised von Mises matrix micro-stress distribution under transverse shear (i.e. $\sigma_{vM}/\hat{\sigma}_{23}$): (a) carbon/E-glass/epoxy RVE and (b) carbon/hollow-E-glass/epoxy RVE.

4 CONCLUSIONS

In this study, a 3D RVE model is developed for intra-laminar fibre hybrid unidirectional composite laminae by generating microstructures with a modified RSE algorithm—accommodating random fibre distributions. The 3D RVE model is initially used to analyse carbon/epoxy ($V_{fC} \approx 0.60$) and E-glass/epoxy ($V_{fE} \approx 0.60$) laminae and is then validated by using the rule of mixture and Halpin-Tsai equations. Subsequently, the RVE model is used to investigate the homogenised properties of and the micro-stress fields in carbon/solid-E-glass/epoxy ($V_{fC} \approx 0.15$, $V_{fE} \approx 0.45$) and carbon/hollow-E-glass/epoxy ($V_{fC} \approx 0.15$, $V_{fH} \approx 0.45$) laminae. With intra-laminar fibre hybridisation, the results show that the effective densities of carbon/solid-E-glass and carbon/hollow-E-glass are considerably altered and that the effective density of carbon/hollow-E-glass/epoxy lamina is comparable to that of carbon/epoxy lamina. Moreover, the longitudinal modulus ($\hat{E}_{11}$) is considerably altered with intra-laminar hybridisation. A higher longitudinal modulus is obtained for carbon/solid-E-glass/epoxy and carbon/hollow-E-glass/epoxy laminae when compared to that of E-glass/epoxy lamina. In addition, a significant increase in the transverse Poisson's ratio ($\hat{\nu}_{23}$) is observed in carbon/hollow-E-glass/epoxy lamina because of the hollow fibre content. In comparison with the specific properties of E-glass/epoxy lamina, the results indicate that the hollow fibre content can considerably lower the specific transverse elastic properties ($\hat{E}_{22}/\hat{\rho}$, $\hat{E}_{33}/\hat{\rho}$ and $\hat{G}_{23}/\hat{\rho}$), while having a negligible effect on the major Poisson's ratios ($\hat{\nu}_{12} = \hat{\nu}_{13}$). In contrast, the specific longitudinal elastic modulus ($\hat{E}_{11}/\hat{\rho}$), and the specific longitudinal shear modulus ($\hat{G}_{12}/\hat{\rho} = \hat{G}_{13}/\hat{\rho}$) are considerably increased. The normalised matrix stress distributions in carbon/solid-E-glass/epoxy and carbon/hollow/E-glass/epoxy laminae under transverse tension and transverse shear loading shown that the matrix stress distributions are slightly different as the hollow E-glass fibres redistribute the local matrix stresses because of the hollowness. In addition, the highest stress amplification is at the shortest inter-fibre distance between the hollow fibres.

REFERENCES

[1] Swolfs Y, Verpoest I, Gorbatikh L. Recent advances in fibre-hybrid composites: materials selection, opportunities and applications. Int Mater Rev 2019;64:181–215. https://doi.org/10.1080/09506608.2018.1467365.

[2] Swolfs Y, Gorbatikh L, Verpoest I. Fibre hybridisation in polymer composites: A review. Compos Part Appl Sci Manuf 2014;67:181–200. https://doi.org/10.1016/j.compositesa.2014.08.027.

[3] Katnam KB, Dalfi H, Potluri P. Towards balancing in-plane mechanical properties and impact damage tolerance of composite laminates using quasi-UD woven fabrics with hybrid warp yarns. Compos Struct 2019;225:111083. https://doi.org/10.1016/j.compstruct.2019.111083.

[4] Selver E, Potluri P, Hogg P, Soutis C. Impact damage tolerance of thermoset composites reinforced with hybrid commingled yarns. Compos Part B Eng 2016;91:522–38. https://doi.org/10.1016/j.compositesb.2015.12.035.

[5] Dalfi H, Katnam KB, Potluri P. Intra-laminar toughening mechanisms to enhance impact damage tolerance of 2D woven composite laminates via yarn-level fiber hybridization and fiber architecture. Polym Compos 2019;40:4573–87. https://doi.org/10.1002/pc.25325.

[6] Yuan YC, Yin T, Rong MZ, Zhang MQ. Self healing in polymers and polymer composites. Concepts, realization and outlook: A review. Express Polym Lett 2008;2:238–50. https://doi.org/10.3144/expresspolymlett.2008.29.

[7] Trask RS, Bond IP. Biomimetic self-healing of advanced composite structures using hollow glass fibres. Smart Mater Struct 2006;15:704–10. https://doi.org/10.1088/0964-1726/15/3/005.

[8] Dalfi H, Al-Obaidi AJ, Razaq H. The influence of the inter-ply hybridisation on the mechanical performance of composite laminates: Experimental and numerical analysis. Sci Prog 2021;104:003685042110232. https://doi.org/10.1177/00368504211023285.

[9] Priyanka P, Mali HS, Dixit A. Mesoscale Numerical Characterization of Kevlar and Carbon–Kevlar Hybrid Plain-Woven Fabric Compression Behavior. J Mater Eng Perform 2019;28:5749–62. https://doi.org/10.1007/s11665-019-04306-6.

[10] De Menezes EAW, Eggers F, Marczak RJ, Iturrioz I, Amico SC. Hybrid composites: Experimental, numerical and analytical assessment aided by online software. Mech Mater 2020;148:103533. https://doi.org/10.1016/j.mechmat.2020.103533.
[11] Banerjee S, Sankar BV. Mechanical properties of hybrid composites using finite element method based micromechanics. Compos Part B Eng 2014;58:318–27. https://doi.org/10.1016/j.compositesb.2013.10.065.
[12] Nemat-Nasser S, Hori M. Micromechanics: Overall Properties of Heterogeneous Materials. Elsevier; 2013.
[13] Xia Z, Zhang Y, Ellyin F. A unified periodical boundary conditions for representative volume elements of composites and applications. Int J Solids Struct 2003;40:1907–21. https://doi.org/10.1016/S0020-7683(03)00024-6.
[14] Yang L, Yan Y, Ran Z, Liu Y. A new method for generating random fibre distributions for fibre reinforced composites. Compos Sci Technol 2013;76:14–20. https://doi.org/10.1016/j.compscitech.2012.12.001.
[15] Hill R. Elastic properties of reinforced solids: Some theoretical principles. J Mech Phys Solids 1963;11:357–72. https://doi.org/10.1016/0022-5096(63)90036-X.
[16] Drugan WJ, Willis JR. A micromechanics-based nonlocal constitutive equation and estimates of representative volume element size for elastic composites. J Mech Phys Solids 1996;44:497–524. https://doi.org/10.1016/0022-5096(96)00007-5.
[17] Vaughan TJ, McCarthy CT. A combined experimental–numerical approach for generating statistically equivalent fibre distributions for high strength laminated composite materials. Compos Sci Technol 2010;70:291–7. https://doi.org/10.1016/j.compscitech.2009.10.020.
[18] Crack initiation and propagation in materials with randomly distributed holes - ScienceDirect n.d. https://www.sciencedirect.com/science/article/pii/S0013794497000398 (accessed April 21, 2023).